Quasi-cleavage hydrogen-assisted cracking path investigation by fractographic and side surface observations

E.D. Merson[1], P.N. Myagkikh[1], V.A. Poluyanov[1], D.L. Merson[1], A. Vinogradov[2]

[1]*Institute of Advanced Technologies, Togliatti State University, Belorusskaya str. 14, Togliatti 445667, Russian Federation*

[2]*Department of Mechanical and Industrial Engineering, Norwegian University of Science and Technology – NTNU, N-7491 Trondheim, Norway*

Abstract

Despite recent substantial advances in understanding of hydrogen embrittlement (HE), many important aspects of this widespread phenomenon remain a subject of debates. Particularly, remarkably different opinions have been expressed on the nature of hydrogen-assisted cracking (HAC), which produces quasi-cleavage (QC) fracture surfaces in iron and low-carbon steels. Basically, two conflicting groups of theories are distinguished concerning causes the QC phenomenon: brittle cleavage-like models and ductile models exploiting localized ductile micro- or nanovoid concepts at the core. The present study was aimed at gaining a new insight into the QC mechanism through the detailed investigation of the HAC path by the microscopic observations of the side and fracture surfaces of the annealed low-carbon steel, which was tensile tested in the ex- and in-situ cathodic hydrogen charged conditions. Using a combination of the scanning electron microscopy, confocal laser scanning microscopy and electron-backscattering diffraction, it was found that the in-situ charging is more suitable for the investigation of HAC by side surface observations because it provokes QC cracking on the side surface and suppresses normal ductile fracture. As opposes to this, HAC after ex-situ charging occurs mainly internally. In this condition, HAC interferes with the normal ductile fracture on the side surface. It is established that the path of secondary QC cracks in the in-situ charged specimen is determined predominantly by the local stress distributions. This holds even on the scale of individual grain. Large deviations of the quasi-cleavage cracks paths from the specific crystallographic planes are found and explained. Nano-voids are regularly observed at the crack tips. Thus, the nano-voids coalescence is supposed to be an integral part of QC HAC.

1. Introduction.

Many metallic materials suffer from substantial degradation of mechanical properties upon interaction with hydrogen. In particular, the drop of ductility caused by hydrogen can result in a dramatic reduction of service life and sudden failures of metallic structures. This phenomenon commonly known as hydrogen embrittlement (HE) remains an essential problem for oil, gas, aerospace, nuclear energy and many other key industries for years. Although a lot of efforts have been made to combat the HE problem and alleviate the harmful hydrogen influence, the challenge still remains because of insufficient understanding of the HE nature and the mechanisms governing hydrogen-assisted cracking (HAC). Despite the vast number of publications in the field and the abundance of accumulated experimental data, many important aspects and details of the HAC process are still missing or unclear. One of such open issues is the nature, and the formation mechanism of the so-called quasi-cleavage (QC) fracture surfaces [1] also referred to as "cleavage-like" [2] or "quasi-brittle" [3], which are found frequently in hydrogen embrittled materials. There is a strong belief that the fracture surfaces of this kind are unique because they possess specific features distinguishing them from all other kinds of fracture surfaces including true cleavage and "original" QC [4,5]. The latter refers to as a fracture surface which is produced by a cleavage crack propagating through the complex microstructure where the perfect cleavage facets cannot be formed [6]. This is the normal brittle fracture mode for many materials [7–10], e.g. some martensitic steels, and, therefore, it is not necessarily connected with HE. In contrast, in the present study, the term QC will be used to designate the specific transgranular faceted fracture surfaces, which are formed at room temperature in hydrogen charged bcc iron and steels with simple microstructures, such as ferrite or ferrite-pearlite. In the absence of hydrogen and at normal conditions such materials demonstrate ductile microvoid coalescence (MVC) fracture. However, below the ductile-to-brittle transition temperature, they break by cleavage with the formation of classical brittle cleavage facets.

The most distinct feature of QC facets is the wide assortment of plasticity markings on their surface, including striations oriented perpendicular to the crack growth direction, straight or Y-shaped ridges with or without the saw-teeth ligaments on their tops, slip lines, etc. [1,4,11–14]. All these morphological elements provide a markedly higher roughness and more ductile appearance of the QC fracture surface, in comparison with true cleavage. These ductile features reasonably prompted the idea about the important role played by plasticity in the formation mechanism of the QC surface. Using the focused ion beam, Martin et al. [1] cut the QC facet, exhibiting a batch of parallel straight tear ridges, and found that intersecting slip bands just beneath the fracture surface were parallel to the slopes of the tear ridges. The authors supposed that such

fracture surface relief is formed by void nucleation at the intersection of slip lines followed by their growth and ductile coalescence in a ductile manner. Hydrogen in this scheme was supposed to promote the formation of the dislocation structure and to enhance void initiation and growth through dislocation processes. This mechanism is consistent with the hydrogen-enhanced localized plasticity (HELP) theory described in details elsewhere [2,15,16]. Lynch [2] proposed the adsorption-induced dislocation emission mechanism (AIDE) according to which hydrogen adsorbing on the crack surface reduces the surface energy so that the HAC occurs mainly by enhanced emission of dislocations from the crack tip and its coalescence with nano-voids ahead of the crack. It was suggested that the striations parallel to the crack front on the resulting QC fracture surface are formed along the lines of intersection of active slip planes. With the use of atomic-force microscopy, Neeraj et al. [17] observed the nano-sized dimples on the QC facets in hydrogen embrittled low-carbon steel. To explain the origin of such a relief, the authors proposed the nanovoid coalescence (NVC) mechanism based on the hydrogen-stabilized vacancy damage accumulation [18] and localized plasticity mechanisms. Based on these premises, these authors suggested that the dimpled QC fracture surface formed as a result of coagulation of vacancies, which are nucleated in the localized plastic zone ahead of the crack tip and are stabilized by hydrogen. The formation of the plastic zone, in this case, is believed to be enhanced through the HELP mechanism.

As an alternative option for the aforementioned “ductile” models, the group of “brittle” theories has been proposed [12,19]. The common underlying idea behind this latter group of theories is that the QC fracture surface results from the normal cleavage cracking promoted by hydrogen, while the ductile features of QC morphology are attributed to concomitant plasticity processes. Using the acoustic emission method, Chen and Gerberich [19] found that QC HAC in single crystal specimens of Fe-3%Si occurred in a discontinuous manner. These authors concluded that the elementary act of HAC includes a cleavage crack jump through the hydrogen-enriched region followed by the crack arrest and blunting until the critical hydrogen concentration ahead of the crack will be again accumulated, and the new brittle crack advancement will occur. This process results in the formation of the QC fracture surface composed of a series of planar segments with crack arrest markings in between. The role of hydrogen in this mechanism is to promote cleavage by the reduction of interatomic bonds – the mechanism known as hydrogen-enhanced decohesion (HEDE) [2,16], or by the restriction of the dislocation emission from the crack tip [20].

It is timely to recall that according to the proposed “brittle” mechanisms, QC HAC should occur strictly along the cleavage planes, which have the {001} orientation primarily in bcc iron and steels. In contrast, the “ductile” mechanisms allow for significant deviations of the crack path from the low-index crystallographic planes at some conditions, which will be considered in the

discussion section of the present paper. Thereby, the crystallographic orientation of the QC fracture surfaces and the HAC path is of great interest.

Even a brief literature survey will disclose that the crystallography of QC is a quite debatable and confusing issue. Tetelman and Robertson [21] for the first time showed that the hydrogen-induced cracks (HICs) in Fe-3%Si single crystals have the {001} orientation coinciding with the cleavage planes in this material. The {001} crystallography of HAC in [100] oriented Fe-3%Si single crystals was frequently confirmed later by other researchers [12,19,22,23]. However, Bernstein et al. [4,24,25] showed that, in contrast to Fe-3%Si, HICs in pure iron were aligned with {110} and {112} planes, while their fracture surface appearance had distinct features differing these HICs from cleavage cracks in Fe-3%Si. Kimura and Kimura [26] found that at temperatures between 200 and 260 K, hydrogen charged pure iron single crystals fractured with the formation of the QC fracture surface having the uncertain orientation, while the {100}, {110} and {112} cleavage facets were found after testing at 170 K. Takano et al. [27] reported that both {100} and {110} oriented fracture surfaces fragments co-existed in the same hydrogen charged pure iron single crystalline specimen with the [100] axial orientation tensile tested at 205 K. Birenis et al. [28,29] observed the (100) QC hydrogen-assisted fatigue crack growth in polycrystalline iron. The QC facets aligned with {110} planes were found in steels with the upper bainite [5] and ferrite [30] microstructure. Merson et al. [11] showed that the average misorientation angle of QC facets in hydrogen embrittled low-carbon steel was twice lower than that for the cleavage facets in the same steel fractured in liquid nitrogen.

Thus, a large number of studies indicates that the crystallographic orientation of the QC fracture surface in iron and ferritic steels can be different from the most commonly anticipated {001} orientation of cleavage planes. Moreover, the considerable roughness of the fracture surface and the non-planarity of the crack path have been observed in hydrogen embrittled iron [24,27]. Recently, using confocal laser scanning microscopy (CLSM), it was shown that QC facets in hydrogen charged low-carbon steel do not necessarily have to be as flat as the cleavage ones; rather they had smoothly curved profiles [11], indicating significant deviations of the crack path from any specific crystallographic plane. The aim of the present paper is to investigate the deviation of the QC crack path from specific crystallographic planes and to clarify the mechanism of QC HAC in the low-carbon steel by thorough side and fracture surface examination using a combination of complementary microscopic techniques - scanning electron microscopy (SEM), CLSM and electron-backscattering diffraction (EBSD).

The observation of a crack on a side surface provides an opportunity to investigate the crack path with respect to the grain microstructure. For successful implementation of such an observation, the necessary prerequisite is that HAC should occur on the side surface. Our previous

works [11,14,31] showed that tensile testing of the ex-situ hydrogen charged unnotched specimens results in the formation of fisheyes – the round shaped regions of the QC morphology surrounded by a normal dimpled relief on the fracture surface. In such a case, the side surface observation of crack growth is difficult because HAC occurs mainly internally. Besides, HAC can interfere with the normal MVC ductile fracture, particularly on the side surface. Therefore, distinguishing between the individual processes underlying each mechanism can be quite challenging. In the present study, the in-situ hydrogen charging was utilized to stimulate the HAC initiation at the surface of the specimen and minimize the contribution of normal MVC during the whole test. The hydrogen-free and ex-situ hydrogen charged specimens were studied as well for the reference.

2. Experimental

Commercially available hot-rolled low-carbon steel grade S235JR with the chemical composition presented in Table 1 was used. The flat rectangular specimens (60×11×2 mm^3), Fig. 1, with a center through-notch were cut along the rolling direction by spark erosion. The notch was introduced to the specimens to evaluate the influence of non-uniform stress field on the HAC path. The specimens were grounded by emery paper up to #2500 grade and then subjected to vacuum annealing at 950 °C for 30 min followed by cooling down in vacuum along with the furnace After annealing, the investigated steel has a typical coarse grain ferrite-perlite microstructure as is described elsewhere [11]. Finally, one face of each specimen was additionally polished with the 1 μm suspension and electrolytically polished around the notch.

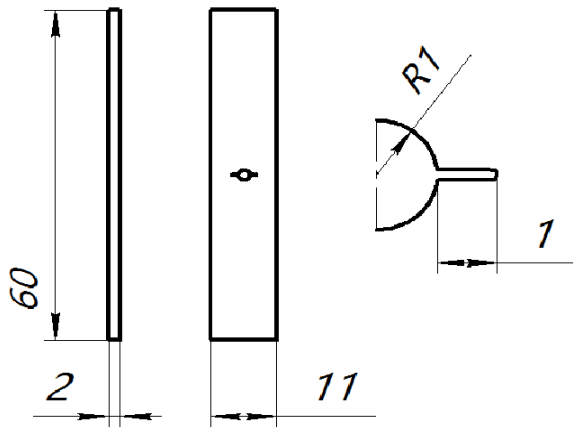

Fig. 1 – The shape of the through-notched specimens used for tensile testing.

Table 1. Chemical composition of the steel S235JR.

Element	C	Cu	Si	Mn	P	S	Cr	Ni	Al	Fe
Wt (%)	0.129	0.067	0.02	0.42	0.019	0.015	0.05	0.007	0.028	Balance

The charging conditions were chosen based on the previous extensive experimental work [E. Merson, Title, PhD thesis (Year) http://misis.ru/files/3833/Merson_ED_disser.pdf (in Russian)] where the effect of the current density of ex-situ cathodic hydrogen charging on the hydrogen concentration, fracture surface and mechanical properties of the S235JR steel has been documented in great details. Particularly, it was shown that the increase of the hydrogen concentration in the range from 1 to 60 ppm resulted only in the quantitative change of number and size of fisheyes, while the mechanism of HAC itself was not changed significantly. Therefore, to maximize the number of QC cracks in the bulk and the area QC morphology on the fracture surface, for the purpose of the present work, the high current density of 200 mA/cm^2 was used for the ex-situ charging during 1 h. In-situ hydrogen charging was performed at 5 mA/cm^2 with the use of the electrochemical cell mounted on the middle part of the specimen during tensile testing. The low current density was used to avoid blistering and HIC. As will be seen below, even this low current density was sufficient to produce the 100% QC fracture surface. The platinum anode and the electrolyte containing 5% H_2SO_4 with the addition of 1.5 g/l thiourea were used for both types of hydrogen charging. The uniaxial tensile tests were conducted at room temperature in air at 0.1 mm/min initial crosshead velocity using a screw-driven H50KT (Tinius Olsen) testing machine. In-situ charging and the tensile test were started simultaneously, immediately after introducing the electrolyte into the cell. Thus, no pre-charging occurred before the test. In the case of ex-situ charging tests, the time gap between the end of charging and the beginning of tensile test did not exceed 10 minutes.

The side surface and fractographic examinations have been conducted using field-emission SEM SIGMA (Zeiss) as well as CLSM Lext OLS4000, (Olympus). The EBSD analysis was performed by the EDAX/TSL Hikari-5 detector integrated in the SEM. No additional processing or preparations have been made to the side surface before SEM and EBSD imaging. The cross-sections were prepared by mechanical diamond water-cooled cutting followed by mechanical grinding and polishing with progressively finer abrasives down to 1 μm grade diamond suspension. The final stage of preparation included vibropolishing for 4 hours in the 0.02 μm colloidal silica suspension in the Vibromet (Buehler) polisher.

3. Results

3.1. Reference hydrogen-free specimens

Looking at the loading diagram of the reference hydrogen-free specimens, Fig. 2, one can distinguish between several consequent deformation stages: (i) quasi-elastic stage with the linearly increasing load; (ii) yield (load) drop; (iii) intermediate strain-hardening stage featured by the nonlinear load raise; (iv) the yield plateau where the load is nearly constant; (v) main strain-hardening stage followed by (vi) load decrease due to the primary crack growth. The intermediate strain-hardening stage is uncommon for the loading diagrams of unnotched specimens of the same steel. Apparently, due to the stress concentration in the vicinity of the notch, plastic deformation in this region commences at the lower external load than in the rest of the specimen. Thus, the yield drop and the subsequent intermediate strain-hardening stage are likely associated with plastic deformation of the close-to-notch region, while the yield plateau and the main strain-hardening stage are due to plastic deformation of the whole specimen. The presence of the notch causes the more abrupt stress decrease during final crack growth than at the normal necking stage of the unnotched specimen.

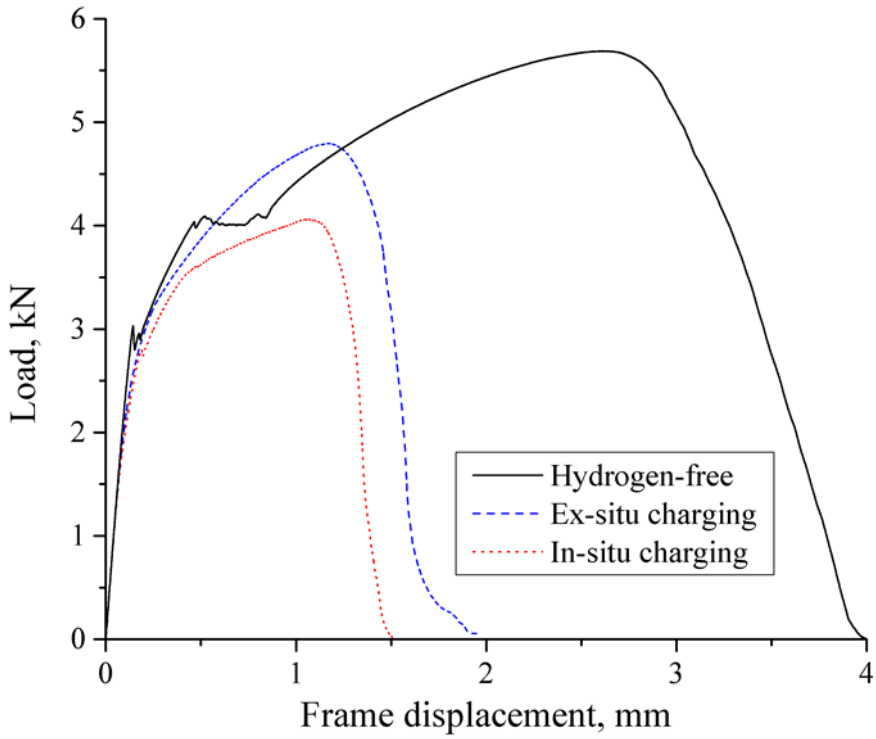

Fig. 2 – The loading diagrams obtained during tensile testing of different specimens.

As is common for mild steels, the hydrogen-free specimen exhibits the completely ductile fracture surface, Fig. 3a, with the typical dimpled relief, Fig. 3b. The side surface of the specimen is covered by numerous voids, ductile microcracks and intersecting slip lines, c.f. Fig. 3c, d. Thus, the fracture of this specimen, which occurred by conventional ductile MVC processes, preceded by significant plastic deformation.

3.2. Ex-situ hydrogen charged specimens

Figure 2 shows that the ex-situ charging results in the decrease of the specimen's elongation and load at fracture. The yield drop and plateau vanish, and the only one characteristic strain hardening stage can be recognized on the loading diagram. Above the load, corresponding to the yield plateau in the reference hydrogen-free specimen, the strain-hardening proceeds at the higher load and rate until fracture. The necking stage is short and the primary crack propagates much faster as follows from the steeper load decay at the end of the test.

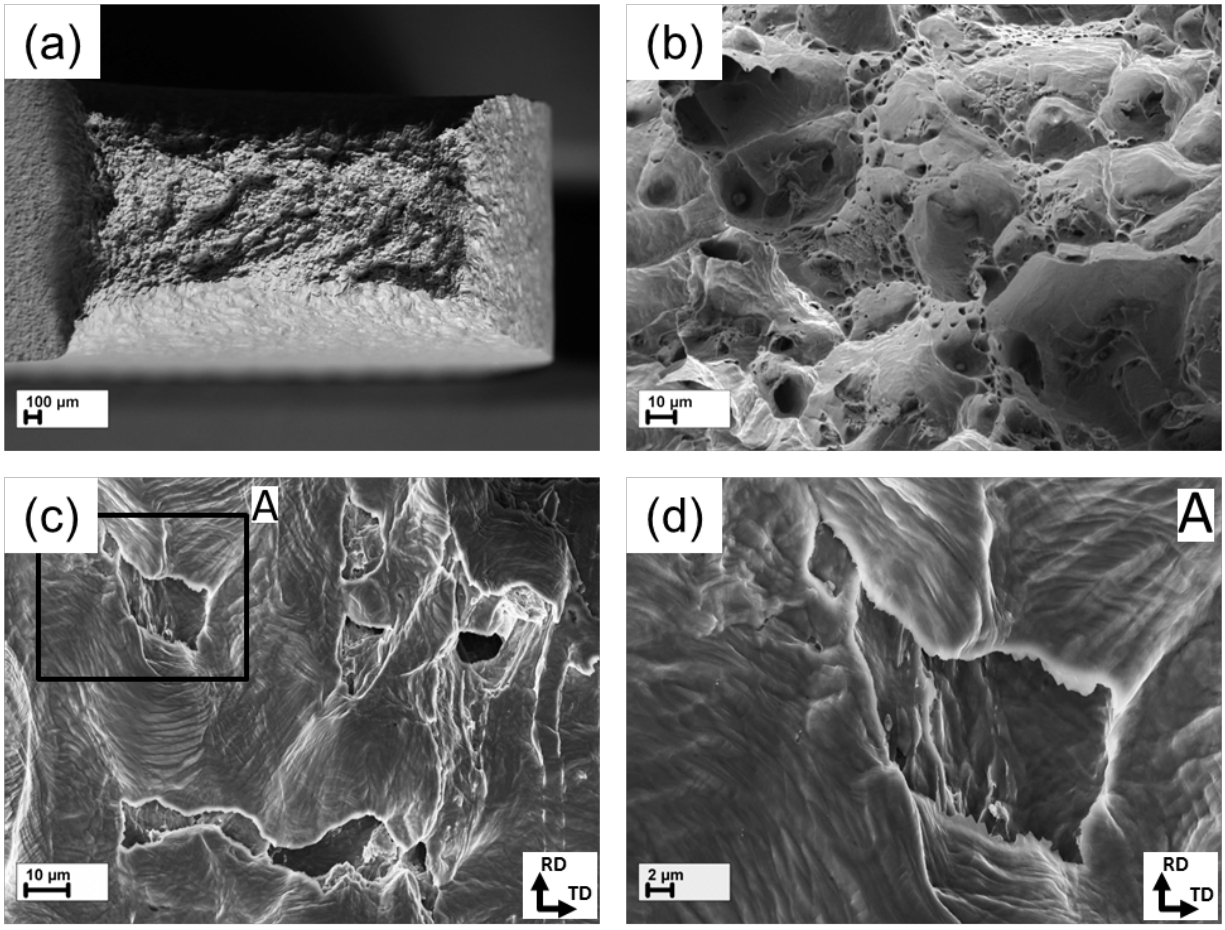

Fig. 3 – SEM images showing the fracture (a, b) and side surface (c, d) of the hydrogen-free specimen after tensile testing: (a) – full-view of a half of the specimen from the notch, (b) –

fragment at the high magnification, (c) – voids and ductile microcracks, (d) – the magnified region marked as “A” in (c).

The microscopic observations show that before the tensile test, the side surface of the ex-situ charged specimen exhibits a vast number of blisters and hydrogen-induced cracks (HICs), such as those shown in Fig. 4a, b. As indicated by surrounding slip lines, Fig. 4b, the formation of these defects during hydrogen charging was accompanied by appreciable plastic deformation. This preliminary plastic strain might be responsible for the elimination of the yield drop and plateau as well as for the rapid increase of the load during the strain hardening stage.

The side surface SEM examination of the ex-situ charged specimen after tensile testing showed many secondary cracks beneath the fracture surface as exemplified in Fig. 4c-f. Despite the brittle-like QC morphology of their inner surface, Fig. 4d, f, which can be occasionally seen, these cracks have a rather ductile appearance when viewed from the side surface. Alike those in the hydrogen-free specimen, the cracks in the ex-situ charged specimen demonstrate ragged edges, wide opening angles, voids and numerous slip lines in between, c.f. Fig. 4c-e. This justifies that the growth of those cracks was accompanied by significant plastic deformation. Nevertheless, on the scale of the whole specimen, the extent of plastic deformation after the tensile test is much less than in the hydrogen-free specimen. This can be clearly seen on the topographic maps in Fig. 5, which were acquired by CLSM from the side surfaces of the specimens. The extent of plastic deformation and the area of the plastic zone under the fracture surface can be assessed by the surface height difference with respect to the undeformed part of the specimen right under the notch. As follows from Fig. 5b, the size of the plastic zone and the surface height difference within this zone are substantially lower than in the hydrogen free specimen, Fig. 5a. Besides, the distribution of plastic strain along the fracture surface of the ex-situ charged specimen is less uniform and is localized mainly in the vicinity of the fracture surface and hydrogen-induced defects.

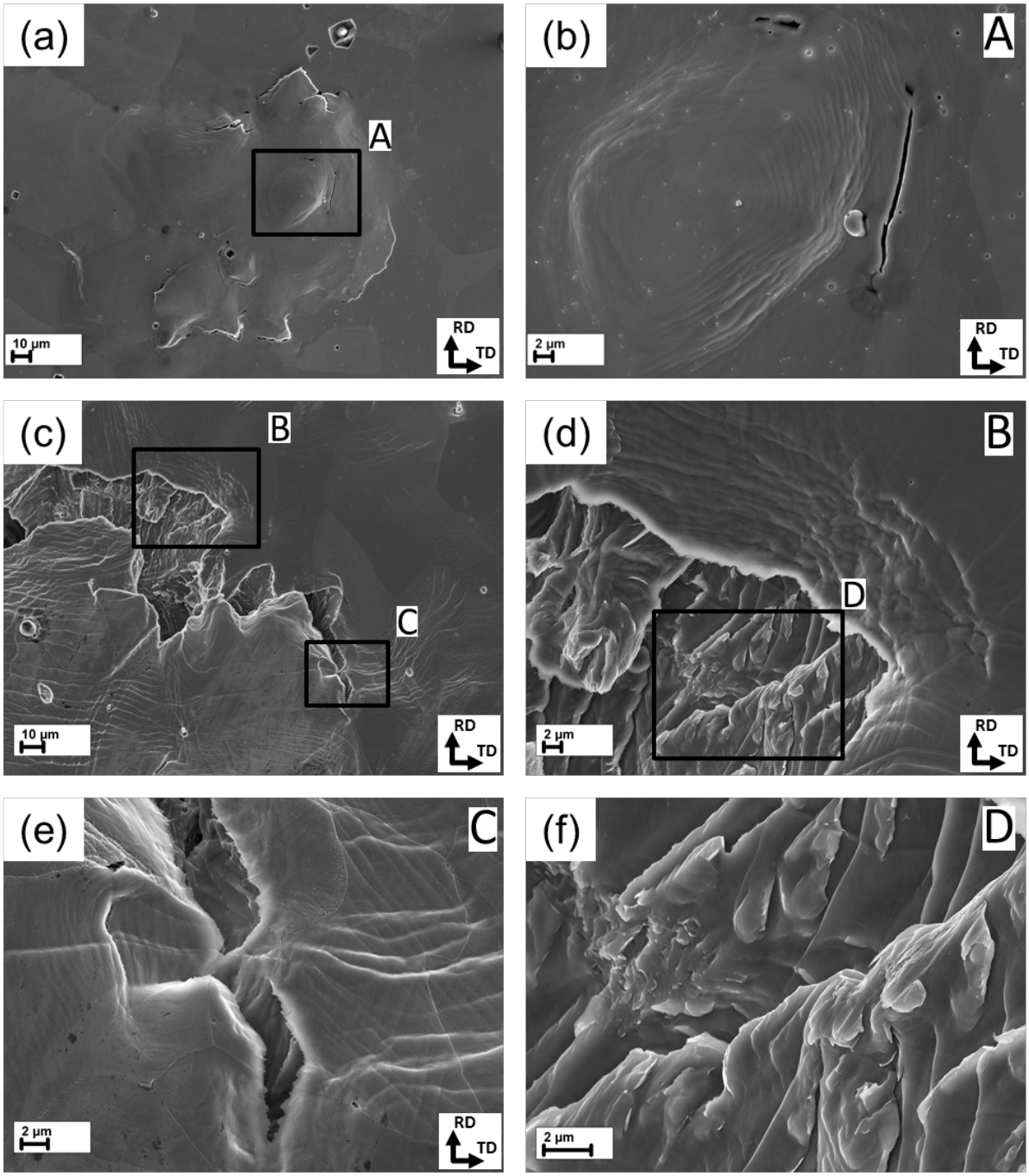

Fig. 4 – SEM micrographs illustrating the side surface of the ex-situ charged specimens before (a, b) and after (c-f) tensile testing: (a) – blister and HICs, (b) – magnified region “A” in (a), (c) – secondary cracks beneath the fracture surface, (d), (e) and (f) – magnified fragments marked as “B”, “C” and “D” in (c) and (d), respectively.

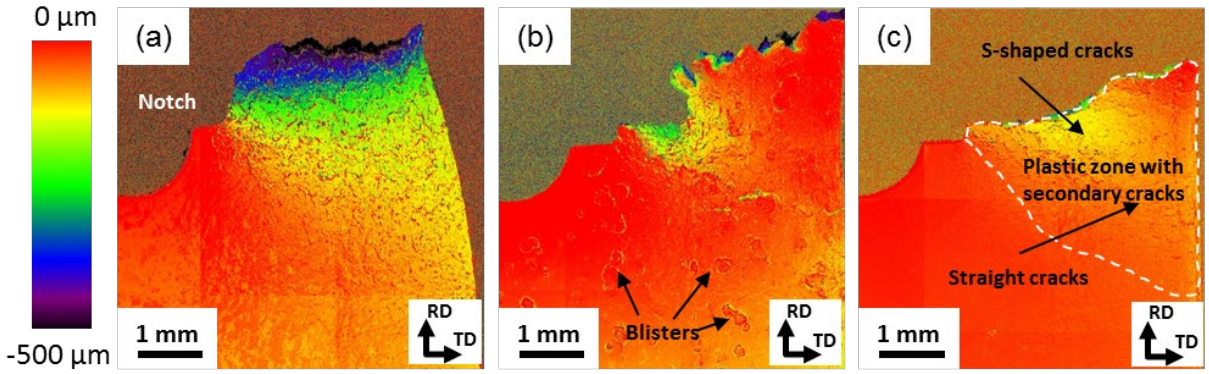

Fig. 5 – The height-colored CLSM maps of the side surfaces of the hydrogen-free (a), ex-situ (b) and in-situ charged specimens (c) after tensile testing. The images represent the regions under the fracture surface of the one half of the specimen from the one side of the notch.

The fracture surface of the ex-situ charged specimens is presented by fisheyes, surrounded by the ductile dimpled relief, c.f. Fig. 6a-d. The surface of the fisheyes has the faceted QC morphology with the distinctive features such as the ridges with the planar or nearly planar regions between them and the steps or striations perpendicular to the ridges, c.f. Fig. 6e, f. The morphology of QC facets and the mechanism of their formation will be considered in more details in the forthcoming publication.

It is known that fisheyes are produced by HACs, which commonly originate at non-metallic inclusions and expand radially along the normal plane with respect to the tensile axis of the specimen [14]. The fractographic analysis shows that, most of the fisheyes nucleated at the cracks oriented perpendicularly to the fracture surface, Fig. 6b. Such cracks are not found in the microstructure and on the fracture surface of the hydrogen-free specimens. Hence, these cracks are regarded as HICs, which were produced during hydrogen charging. HICs are known as hydrogen traps containing hydrogen inside their inner volume as well as in the ~50 µm layer around them [32]. Taking into account that these cracks also serve as stress risers, the nucleation of fisheyes at HICs is plausibly expected.

Once nucleated, the fisheyes extend radially from the initiation sites. However, they almost never exit at the side surface. Even when they approach the side surface very closely, the narrow streak of the dimpled relief always appears between the fisheye and the surface, Figs. 6b,d. Undoubtedly, plastic deformation and MVC processes preceding the formation of this ductile fracture surface affected the side surface morphology. Therefore, most of the ductile features, which are observed on the side surface of the ex-situ charged specimen, Figs. 4c-f, cannot be immediately attributed to HAC. This substantially complicates revealing the HAC mechanism by the side surface observations in the ex-situ charged specimen.

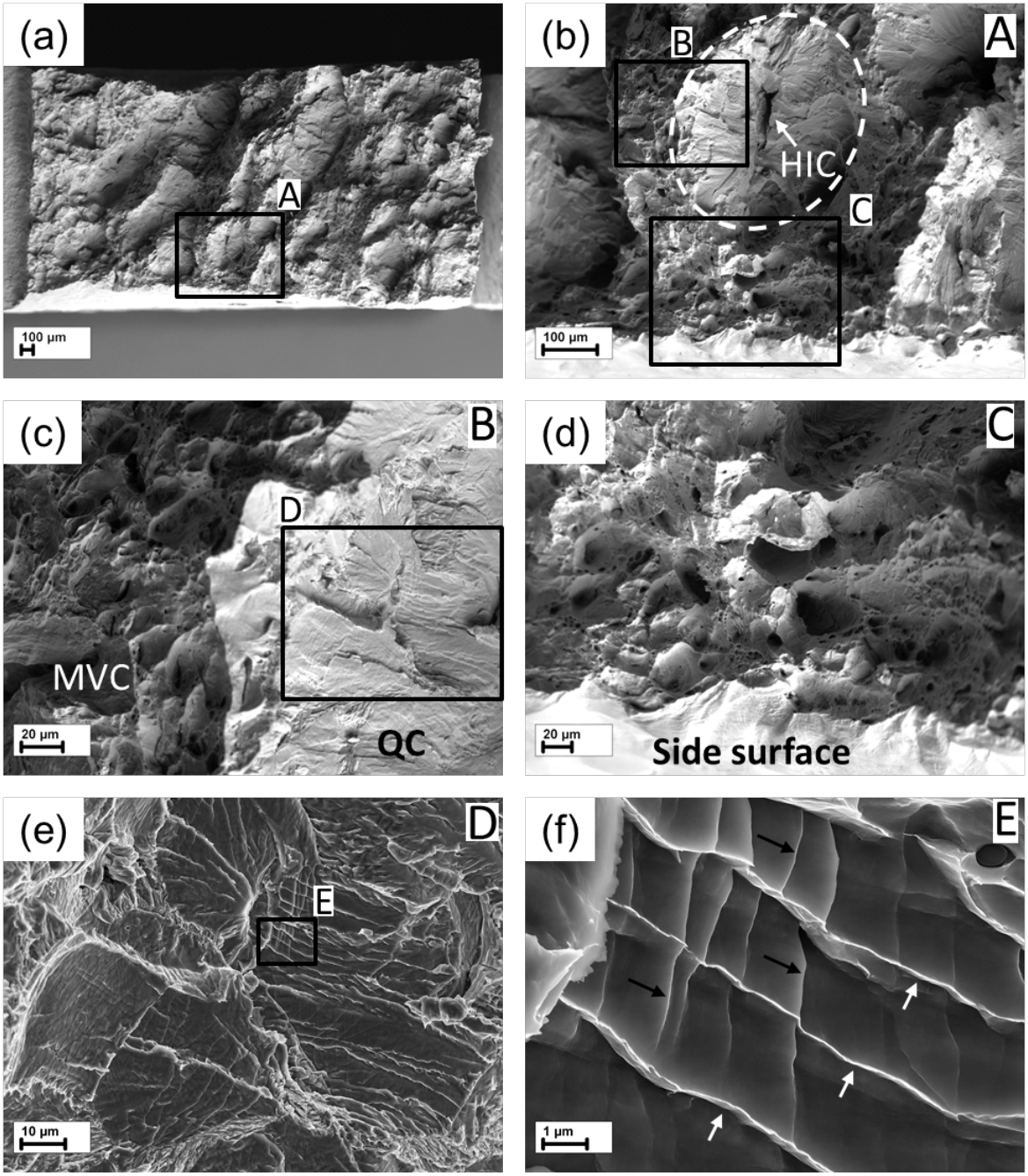

Fig. 6 – The fractographic features of the ex-situ charged specimen: (a) – full view, (b) – the magnified fragment "A" in (a) representing fisheye (depicted by dotted line) with the HIC in the center, (c) – the magnified region "B" in (b) representing transition from fisheye's QC to dimpled MVC fracture, (d) – the magnified region "C" in (b), representing dimpled streak between the fisheye and the side surface, (e) – the magnified fragment "D" in (c) representing QC morphology of the fisheye, (f) – the magnified region "E" in (e) representing ridges (white arrows) with planar areas between them and the perpendicular striations (black arrows).

The cross-section EBSD analysis of the tensile tested ex-situ charged specimen was performed to investigate the path of the internal fisheyes cracks. The clearly transgranular cracks

oriented primarily perpendicular to the tensile axis are found beneath the fracture surface, c.f. Fig. 7. As can be seen on the EBSD inverse pole figure (IPF) coded orientation maps superimposed with the image quality (IQ) map, some of the cracks are ladder-like arranged, Fig. 7a, b while others have a visibly more straight appearance, Fig. 7e. Interestingly that the path of the cracks appears to be insensitive to the crystallographic orientation of the grains. The cracks can cross the grain boundaries without significant deviations of their growth direction, and, on the other hand, they can smoothly curve within one grain having the uniform crystallographic orientation, as illustrated in Fig. 7b. The deviation of the crack path from the specific crystallographic planes is also indicated by the local waviness of the edges of the crack, which can be regularly seen on the finer scale, Fig. 7f. Some of the cracks exhibit the small voids at the tips with distinct ligaments seen as “micro-necks” between the voids, Fig. 7d. The extensive slip accompanied the crack growth as is evidenced by the dense slip lines and local misorientation of the grains at the crack tips and faces, c.f. Fig.7c, d, f.

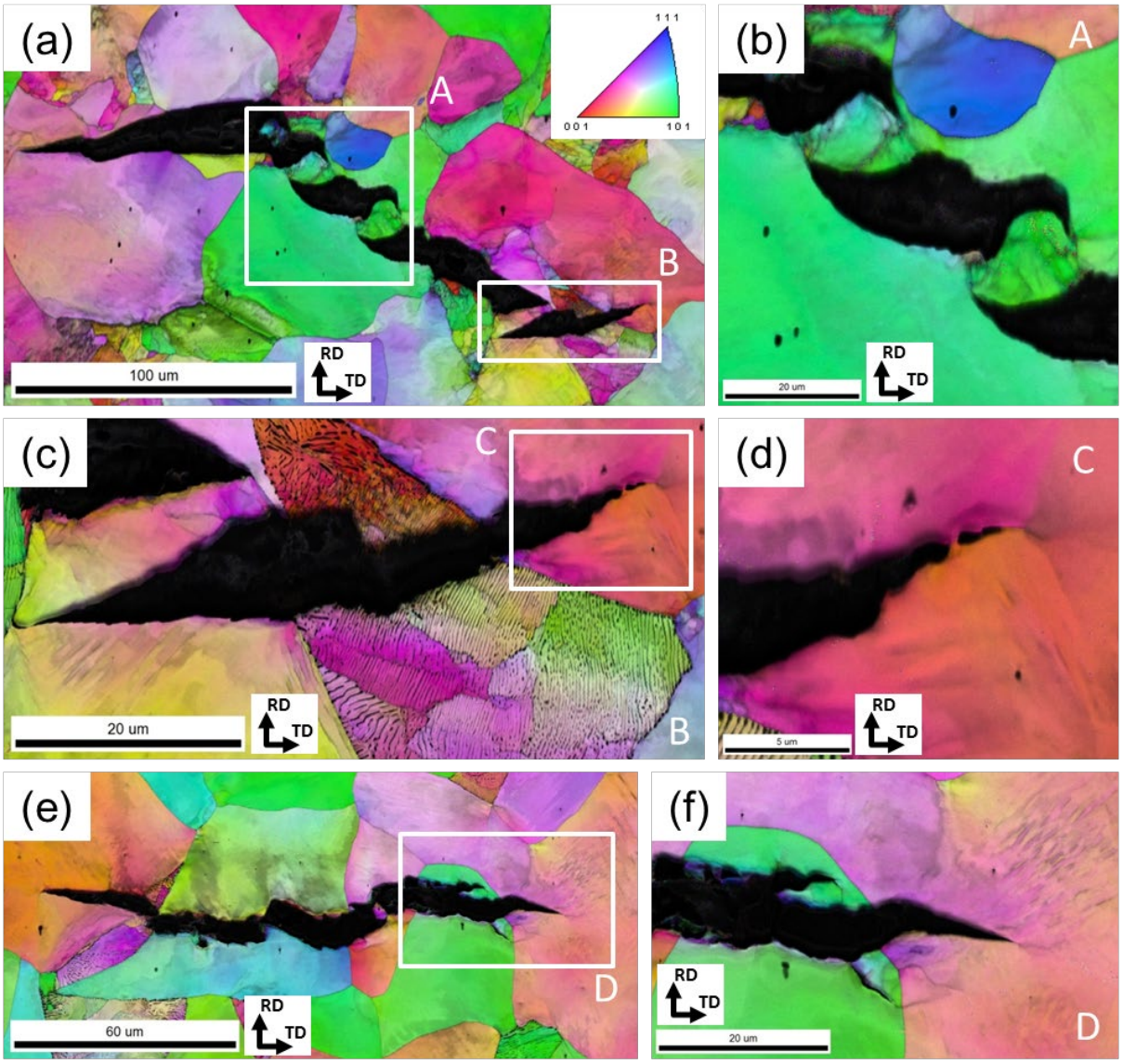

Fig. 7 – The EBSD maps in inverse pole figure (IPF) colors + image quality (IQ) contrast, representing the inner cracks in the cross-section of ex-situ charged specimen after tensile testing: (a) – the ladder-like arranged cracks, (b) – magnified fragment "A" in (a) representing smoothly curved cracks, (c) – magnified fragment "B" in (a) representing the crack passing through the pearlite and ferrite grains, (d) – magnified fragment "C" in (c) representing the crack tip featured by voids and emanating slip lines, (e) – the crack crossing a few ferritic grains, (f) – magnified region "D" in (e) representing the crack with wavy edges and slip lines emanating from the tip. ESBD scanning was performed with the 150 nm step size for (a,b), 50 nm for (c,d) and 120 nm for (e,f).

Although the cracks observed in the cross-section demonstrate rather ductile features, their fracture surface morphology is not clear. As was shown above, the fracture of the ex-situ charged specimen was preceded by pronounced plastic deformation, at least on the local scale. Moreover,

HAC interferes with normal ductile MVC processes. Thus, it cannot be excluded that the observed curviness of the cracks and their ductile features, such as voids, arise from the normal ductile fracture which accompanies the propagation of fisheye cracks. In order to avoid the influence of the normal ductile fracture and to stimulate HAC on the side surface, the test with in-situ hydrogen charging was conducted.

3.3. The specimen tested during in-situ hydrogen charging.

Figure 2 shows that the in-situ charged specimen suffers from the greater decrease of the elongation and load at break than the ex-situ charged one. The loading diagram obtained during in-situ charging exhibits the same deformation stages as the hydrogen-free specimen except for the yield plateau, which ceases to occur in the in-situ charged specimens. The reason for that is not fully clear as yet. Since no blisters and HICs were found in this specimen, the lack of the plateau region is possibly caused by plastic deformation, which is promoted by hydrogen ahead of the notch and which occurs at stresses lower than the upper yield point of the material so that the Lüders band cannot be triggered until final failure. Although the yield plateau does not show up, two distinct strain-hardening regions can be recognized by the inflexion point on the loading diagram at about 3.5 kN, above which the load increase slows down. The small yield drop followed by relatively fast strain-hardening occurs at the lower stress than in the hydrogen-free and ex-situ charged specimens. The stress decrease during final crack growth occurs faster than in the other specimens.

In agreement with expectations, the fracture surface of the in-situ charged specimen is represented solely by the elements characteristic of the QC fracture, Fig. 8a, b. No signatures of the ordinary ductile dimpled relief were found. QC features, in this case, are similar to those of fisheyes in the ex-situ charged specimen. Namely, the ridges, planar segments and striations oriented nearly perpendicularly to the ridges are found on the fracture surfaces of both the ex- and in-situ charged specimens, Fig. 6f and 8c, d. However, it is worth noting that the ridges in the in-situ charged specimen appear more ordered and closely spaced than in the ex-situ charged one.

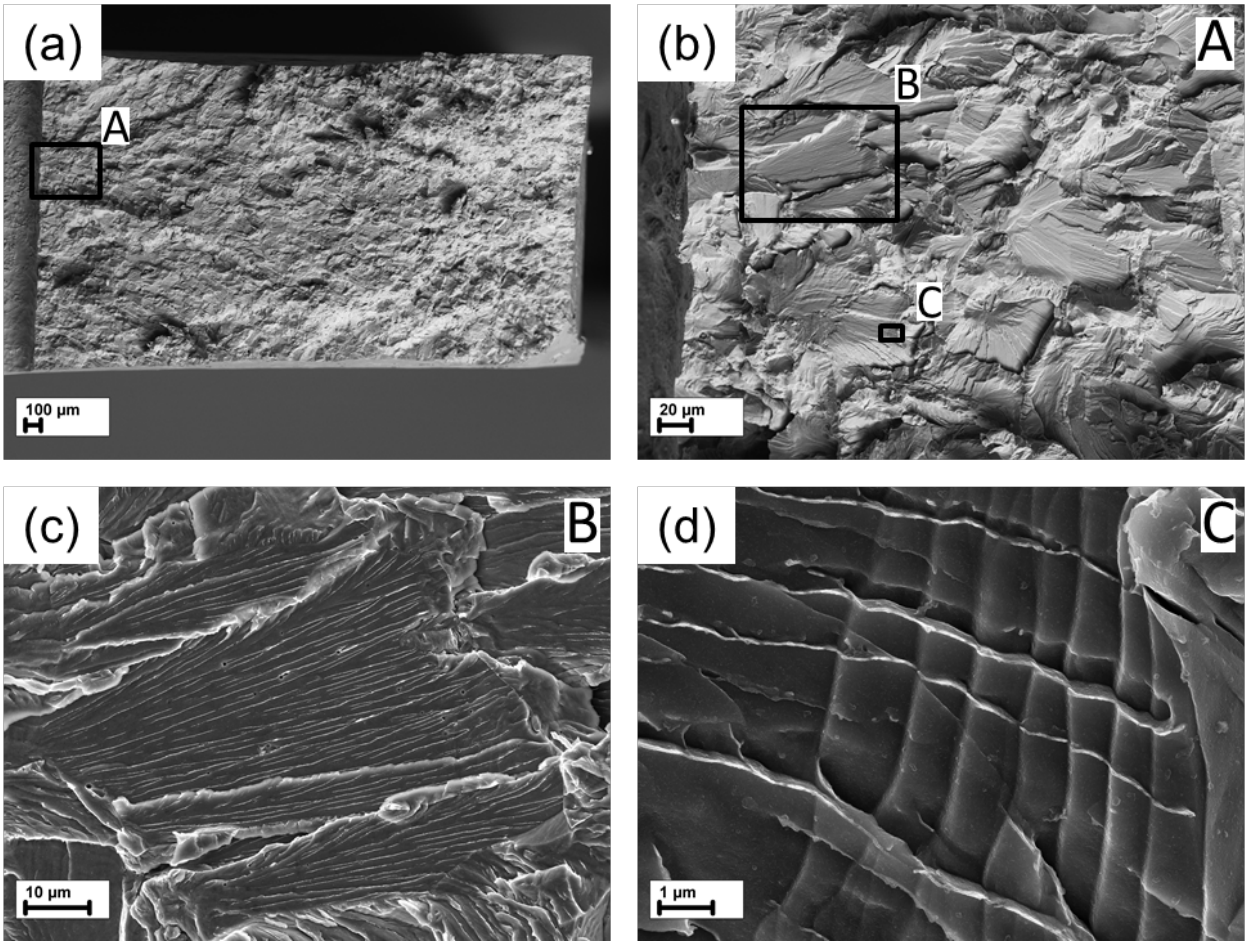

Fig. 8 – The fractographic features of the specimen tensile tested during in-situ hydrogen charging: (a) – full view, (b) – magnified region marked as "A" in (a) representing 100% QC morphology, (c) – the magnified region "B" in (b) representing the QC facet, (d) – the magnified region "C" in (b), illustrating typical ridges, planar segments and steps perpendicular to the ridges on the surface of the QC facet.

Numerous secondary cracks, shown in Fig. 9 and 10, are observed on the side surface of the specimen tested during in-situ charging. All cracks are found only within the plastic zone depicted in Fig. 5c, which size is slightly larger than that in the ex-situ charged specimen, Fig. 5b. Most of the cracks are transgranular, even though many, if not most, of them likely originate at the boundaries between ferritic grains, Fig. 10a or at the interface between the ferritic grain and the cementite lamellas in pearlitic grains, Fig. 10b. The cracks in the specimen tested during in-situ charging are notably narrower and sharper than those in the hydrogen-free and ex-situ charged specimens. Some of them have very thin, hair-like tips with of 20 nm opening, Fig. 11a. The observed blurred contrast of such very sharp tips indicates that their volume is likely not connected with the side surface of the specimen yet. Despite the prima facie brittle appearance of the cracks, the nano-sized voids can be observed inside the open tips at high magnification, Fig. 11c, d. These

voids are evidently produced due to the tearing of a thin membrane between the specimen side surface and the inner volume of the crack. Such walls, which appear as the blunted ligaments between two faces of a crack, are frequently found inside the tips of the cracks, Fig. 11a, b.

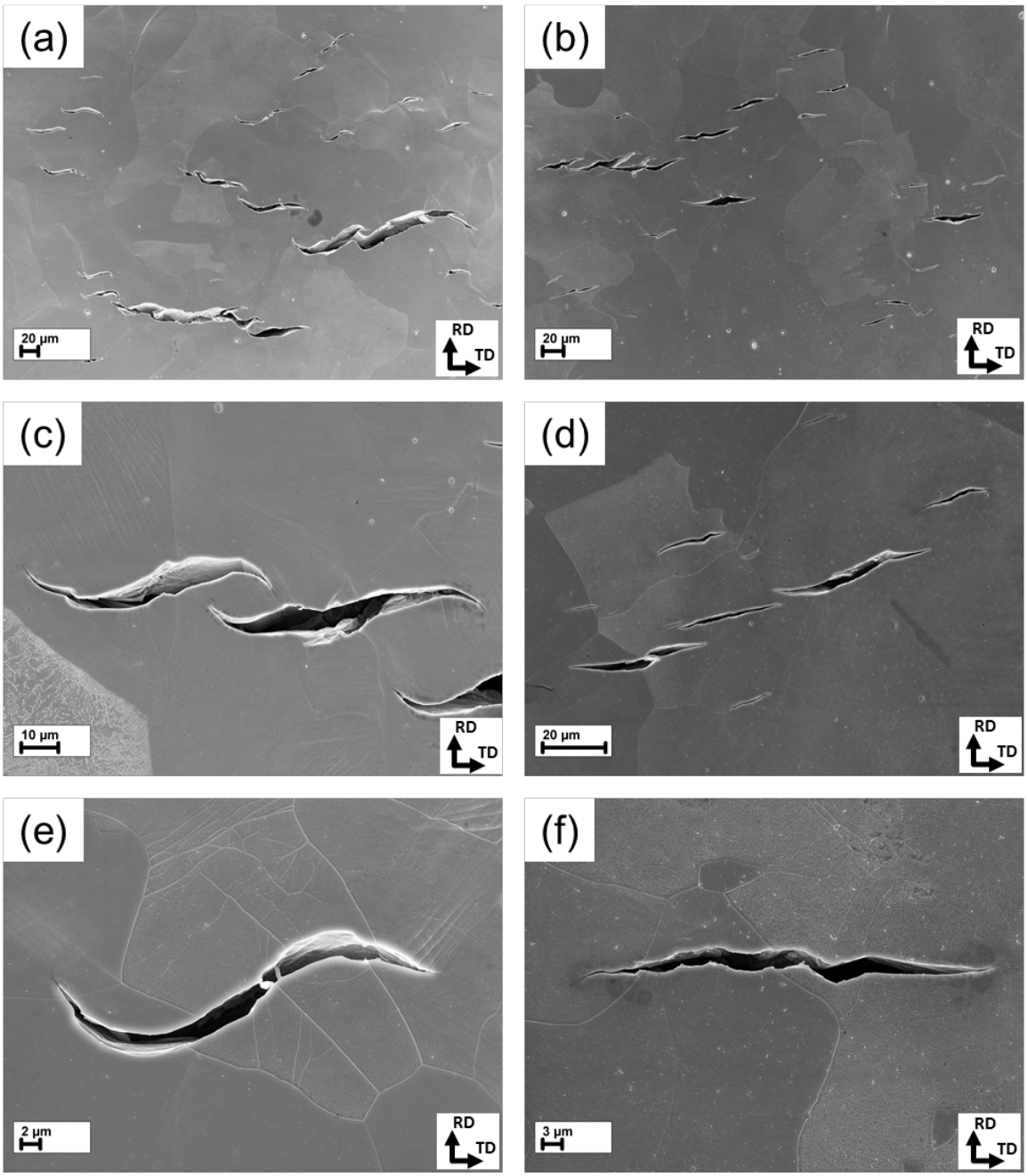

Fig. 9 – The S-shaped (a, c, e) and contingently "straight" (b, d, f) secondary cracks on the side surface of the in-situ charged specimen: (a, b) – the magnified regions marked as "s-shaped cracks" and "straight cracks" in Fig. 5c, (c) – the closely spaced S-shaped cracks arranged in "paragraph sign" (§) – pattern, (d) – the closely spaced "straight" cracks, (e) – the detached S-crack, (f) – the detached "straight" crack demonstrating local waviness on the finer scale within the grain.

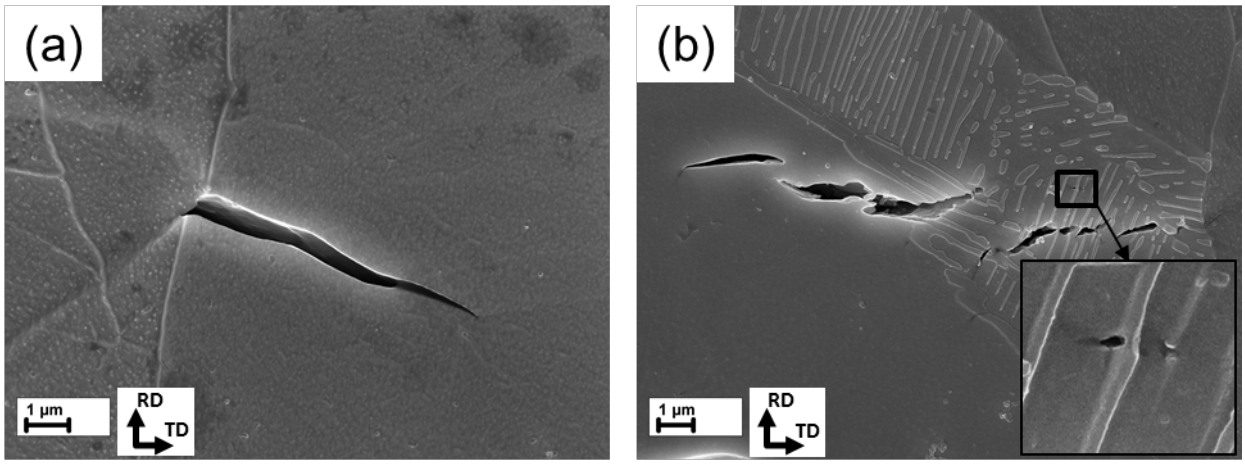

Fig. 10 – The side-surface secondary cracks originating at the boundaries between two ferritic grains – (a) and between ferritic grain and cementite lamellas in a pearlitic grain – (b).

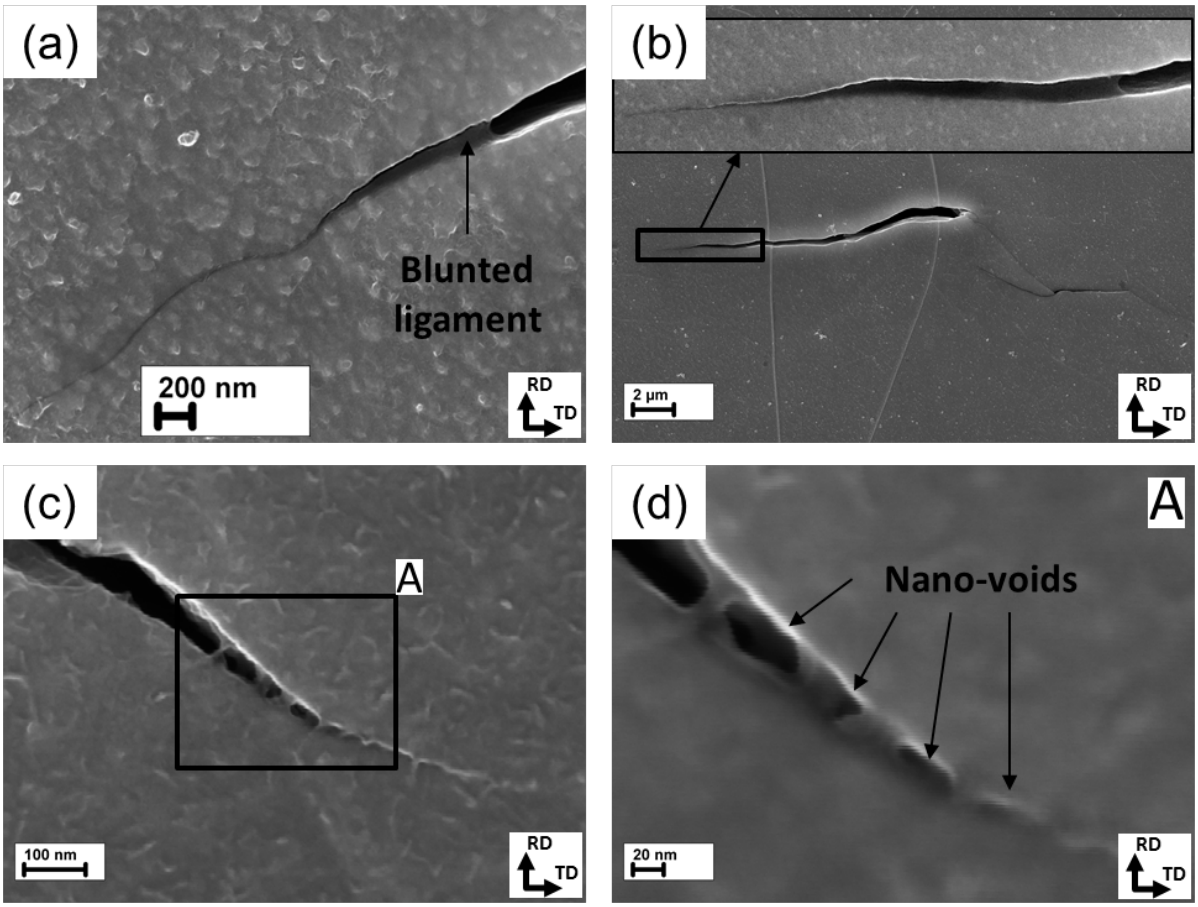

Fig. 11 – The tips of the secondary cracks on the side surface of the specimen tested during in-situ hydrogen charging: (a, b) – the hair-like crack tips with blunted ligaments, (c, d) – the crack tip with nano-voids, (d) – the magnified region marked as "A" in (b).

Many cracks, which are found near the fracture surface, have a specific smoothly curved "S"-like shape, c.f. Fig. 9a, c, e and Fig. 5c. This shape is very similar to that of QC facets profiles

observed on the fracture surface in our previous study [11] as well as to that of the cracks which were found in the cross-section of the ex-situ charged specimen, Fig. 7b. Alike those cracks in the cross-section, the closely spaced S-cracks form a “paragraph sign” (§) - like patterns on the side surface of the in-situ charged specimen, Fig. 9c. This results in the corresponding wavy relief of the fracture surface, such as that shown in Fig. 12.

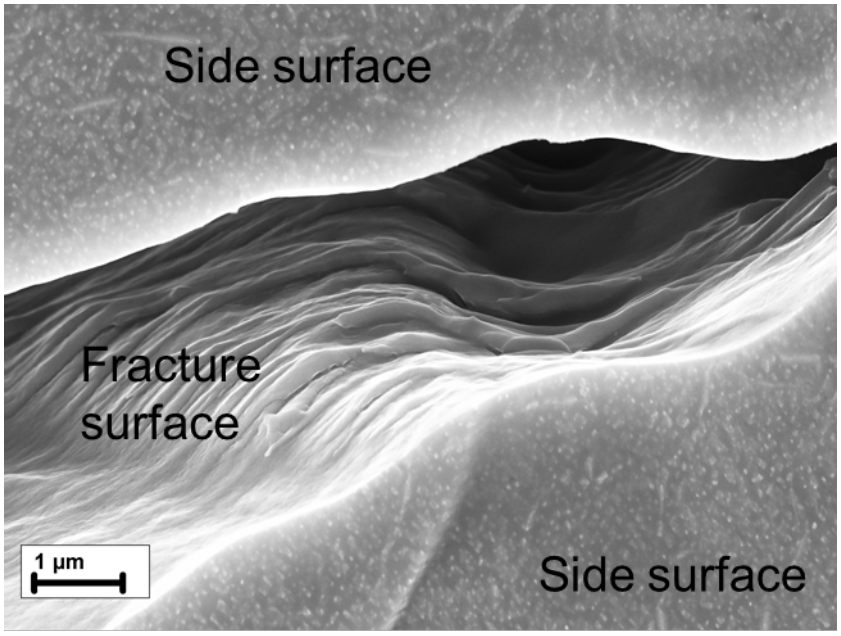

Fig. 12 – Wavy inner surface of the secondary crack viewed from the side surface of the in-situ charged specimen.

The curved shape of the secondary cracks is likely not (or not only) due to their interaction with each other. This is corroborated by two observations. The first is that the individual S-cracks without near neighbors around can be found on the side surface, Fig. 9e. The second is that most of the cracks, appearing in the periphery part of the plastic zone far from the fracture surface, remain quite straight even when they are very close to each other, c.f. Fig. 9b, d, f and Fig. 5c. Thus, the cracks demonstrate a stronger tendency to curve when they appear in the high-stress region which is closer to the notch and to the fracture surface. This implies that the crack path is strongly influenced by the stress field from the notch and from the main crack. The similar conclusion was recently drawn by Laureys et al. [33] who also found the S-shaped cracks in the notched specimens of pure iron tensile tested during in-situ hydrogen charging. Nevertheless, it should be noted that even those contingently straight cracks, which are found far from the notch, exhibit some appreciable waviness on the finer scale, Fig. 9f and 11a.

As a general observation, Figure 9a-d shows that the closely arranged cracks have a quite similar orientation with respect to the tensile axis, even if they nucleate in different grains. This

indicates that the path and orientation of the cracks are more dependent on the stress fields than on the microstructure and crystallographic orientation of grains. The strong evidence for this conclusion is illustrated by the EBSD map in IPF+IQ colors in Fig. 13a, where the S-shaped crack smoothly bends within the individual grain (marked by “B”) having the uniform crystallographic orientation; and at the same time, this crack crosses the boundaries between differently oriented grains (A/B, or C/D) without any significant deviation from its primary growth direction. The traces of {001} (black lines) and {011} (white lines) crystallographic planes are shown in Fig. 13a along the crack path. The traces correspond to the planes which orientation is closest to that of the crack edge in the local region. As can be seen, in general, the path of the crack cannot be fully associated with any particular low-index crystallographic plane, though in some grains or local regions the orientation of the crack is close to specific low-index planes. However, it should be noted that some of the cracks obviously grow along the specific crystallographic planes, e.g. the two cracks in Fig. 13b.

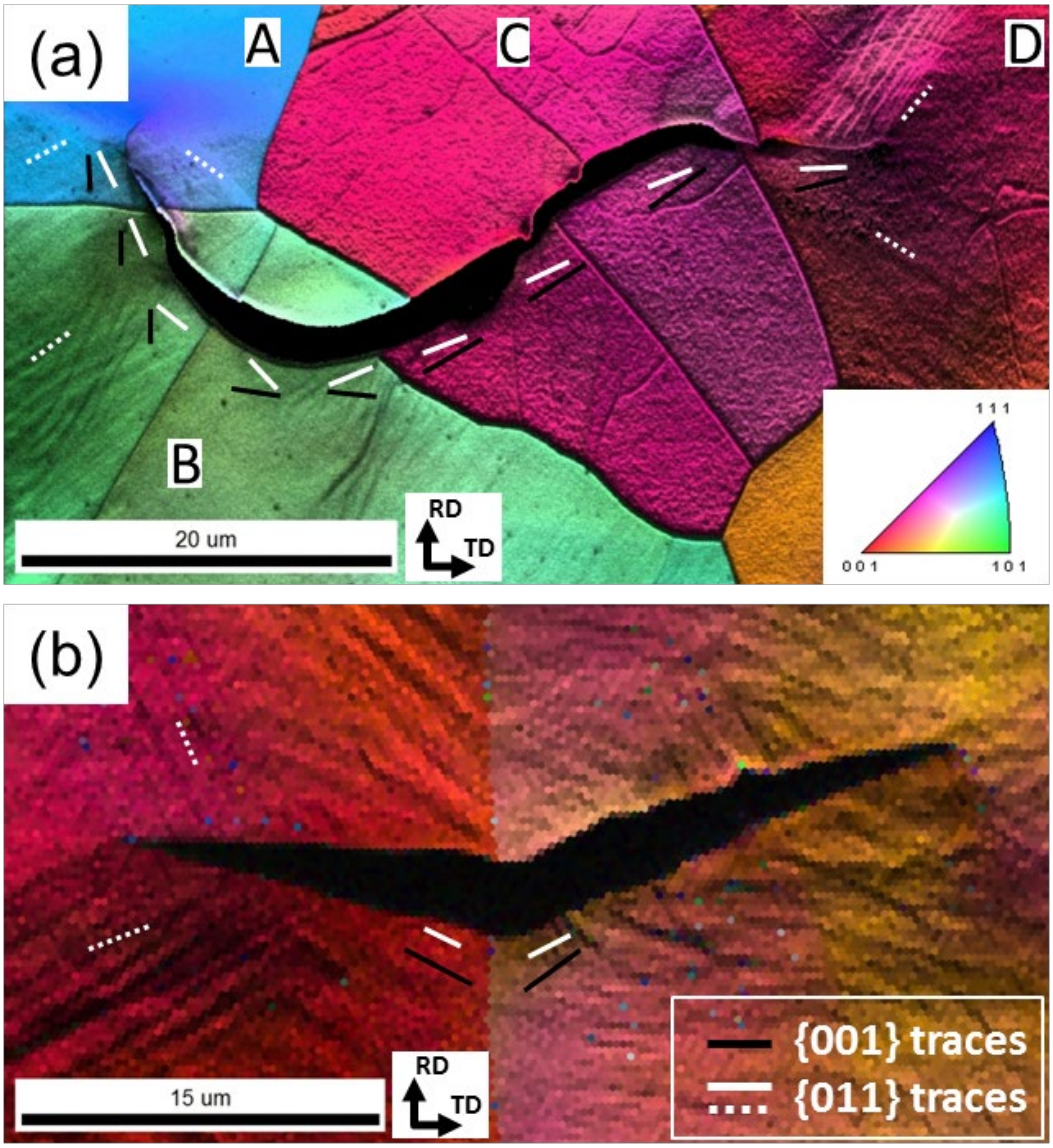

Fig. 13 – The EBSD maps in colors of inverse pole figure (IPF) + image quality (IQ) contrast, representing the secondary cracks on the side surface of in-situ hydrogen charged specimen: (a) – S-shaped crack, which path largely deviates from the low-index crystallographic planes, (b) – the nearly crystallographic straight cracks originated at grain boundaries. The black and white lines indicate the traces of the {001} and {011} crystallographic planes, respectively.

4. Discussion.

4.1. The features of HAC at the ex- and in-situ hydrogen charging.

The obtained results suggest that tensile testing during in-situ charging is more suitable for the analysis of HAC features in low-carbon steel than the ex-situ charging followed by the tensile

loading. The in-situ charging effectively suppresses the normal ductile MVC fracture, thus causing the pure hydrogen-assisted QC fracture in the investigated steel. Besides, it facilitates HAC on the side surface of the specimen, providing an opportunity to investigate the crack path with respect to the microstructure alongside as well as to the fracture surface features. A brief description of the processes resulting in fractographic and side surface features observing at the ex- and in-situ charging is given below and schematically shown in Fig. 14. For simplicity, the scheme in this figure assumes the unnotched geometry of the specimens.

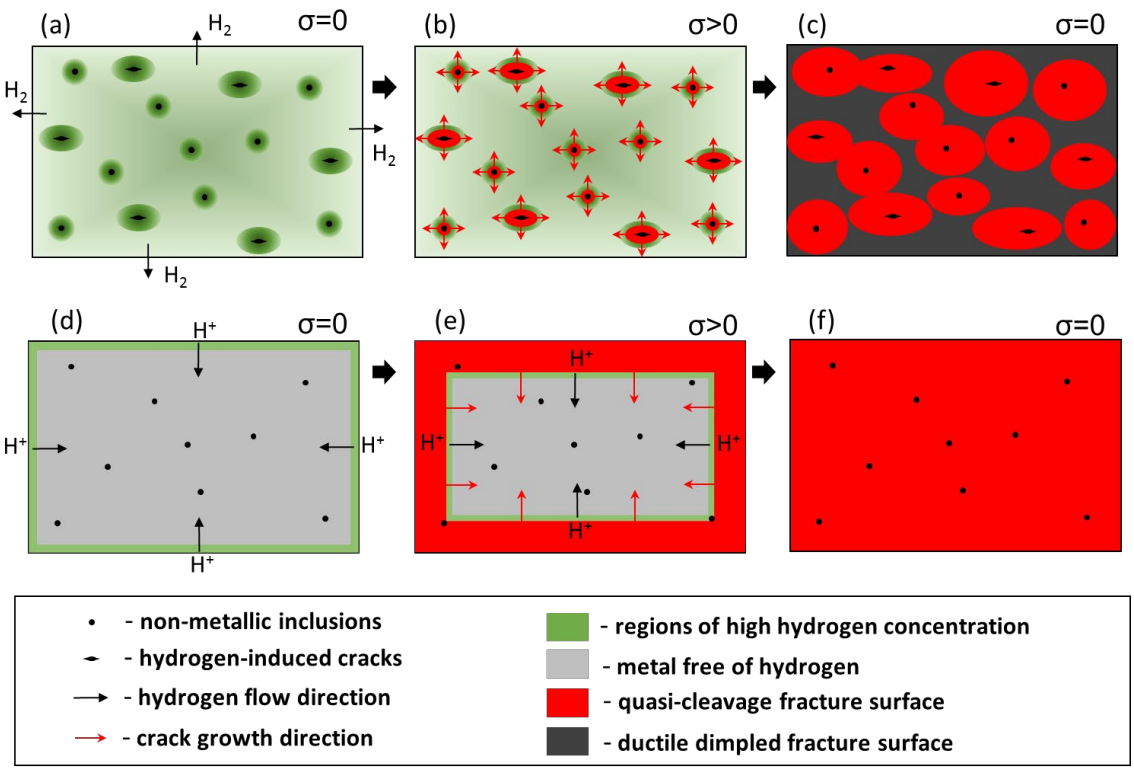

Fig. 14 – The schematic representation of the cross-section (a, b, d, e) and fracture surface (c, f) perpendicular to the tensile axis for unnotched specimens of low-carbon steel before (a, d), during (b, e) and after (c, f) tensile testing at ex- (a-c) and in-situ (d-f) hydrogen charging.

During ex-situ charging, diffusible hydrogen in the form of atoms penetrates into the microstructure of the metal. Hydrogen is distributed in the crystal lattice and over different traps such as dislocations, grain and interphase boundaries, non-metallic inclusions, etc. [34]. The molecular hydrogen can be formed when the hydrogen atoms are met at some discontinuity which has a large enough volume, e.g. at the boundaries between non-metallic inclusions and the matrix. The increasing volume of hydrogen due to recombination of atoms into molecules results in a strong pressure buildup inside the discontinuity, which finally causes HIC and blistering [35,36]. The formation of HICs is accompanied by plastic deformation of the surrounding metal. Thus, the

high concentration of diffusible hydrogen is produced around the HICs because of newly created dislocations serving as effective reversible traps for hydrogen [32]. In the time lag between the end of the hydrogen charging and the start of the tensile test, the excess hydrogen dissolved in the lattice rapidly evolves from the specimen to the atmosphere, while the trapped hydrogen retains in the microstructure, Fig. 14a. During the tensile test, HAC originates at the sites of the highest hydrogen and stress concentration, such as HICs and non-metallic inclusions. The cracks advance in the radial direction from the initiation points, producing round shaped areas of the QC fracture surface – fisheyes, Fig. 14b. The high concentration of atomic hydrogen at the crack tip is pivotal for this process. Hydrogen is supplied to the crack tip region mainly by diffusion, the rate of which depends on the concentration of diffusible hydrogen in the matrix. The contribution of atomic hydrogen, which is reduced on the inner surface from gaseous hydrogen in the crack, is believed to be minor. Due to the gradual increase of the crack front and a limited amount of hydrogen in the specimen, the rate of hydrogen supply to the crack tip region, occasionally, can be too low to maintain the steady crack growth by the QC mode. In this case, the crack either blunts and stops until hydrogen is resupplied to its tip, or grows in the ductile MVC mode if the stress intensity factor at the crack tip is high enough. The latter growth can occur, for example, when the ligament between two fisheyes (or between a fisheye and a side surface of the specimen) is reduced to the critically small thickness and ductile fracture of this ligament proceeds by the normal MVC mechanism. This process causes the formation of the dimpled relief around fisheyes, Fig. 14c, as well as the appearance of ductile cracks and voids on the side surface of the specimen.

The in-situ hydrogen charging was started simultaneously with tensile testing. Since there was no precharging, no hydrogen was introduced into the specimen, and, consequently, no hydrogen-induced defects were formed before the test. Thus, when external stress was applied, the high hydrogen concentration is produced only in the surface layer of the specimen, Fig. 14d. This circumstance causes the HAC to occur from the side surface of the specimen towards the bulk, Fig. 14e. During the test, the high hydrogen concentration is constantly maintained at the crack tip, because of the stable contact of the electrolyte with the specimen surface. Thereby, the cracks propagate steadily by the QC mode only, Fig. 14f.

It is worth noting that the scenarios described above apply the hydrogen concentrations and hydrogen charging conditions which were used in the present study. However, the results of our previous studies allow assuming that the variation of the hydrogen concentration would not affect fundamentally the mechanism of HAC and HIC in the present steel, though the quantitative changes are expected, for example, in the number and the area of fisheyes [37].

4.2. The features of the HAC path in the low-carbon steel.

The obtained results unequivocally show that QC HAC path can be clearly crystallographic, but on the other hand, it may also significantly deviate from the specific crystallographic planes at least on the scale of a single grain. It is quite hard to imagine how the smoothly curved cracks and fracture surfaces, such as those shown in Fig. 9e, 12, and 13a, can by produced by the cleavage mechanism in a ferritic grain. The images obtained in the present study, Fig. 12c, d, indicate that nucleation and coalescence of voids, i.e. the ductile fracture, is the inherent part of the HAC and QC fracture surface formation processes. Thereby, one or few of "ductile" HE mechanisms, namely HELP, AIDE or NVC, can be responsible for QC HAC in low-carbon steel. As will be discussed below, the smoothly curved appearance of cracks can be explained by these mechanisms much easier than by HEDE or other brittle HE mechanisms.

For example, according to the AIDE model, HAC occurs by the emission of dislocations from the crack tip and its coalescence with nano-sized voids in front of the crack tip. This process is facilitated by hydrogen adsorbing on the crack surface, and, thus, causing surface energy reduction. From the fractographic observation, it was concluded that in this way HAC in bcc iron and steels should occur along the low-index crystallographic planes, mainly having the {100} orientation, towards the <110> directions. As was noticed by Lynch, "Macroscopic planes for transgranular cracking would, therefore, bisect the angle between the slip planes, and crack fronts would lie along the line of intersection of crack planes and slip planes, e.g., along {100} planes in ⟨ 110 ⟩ directions when {111} or {112} slip planes were active in fcc or bcc materials" [2]. However, he also noted that "deviations from low-index planes and directions would occur if unequal amounts of slip occurred on either side of cracks owing to large differences in shear stresses on the different slip planes. Deviations of fracture planes away from low- index planes could also occur depending on the location of void." Consequently, the AIDE mechanism allows for both the crystallographic and contingently non-crystallographic crack growth with the later arising "because slip planes on one side of the crack are much more highly stressed than those on the other side that slip occurs preferentially on one side of the crack" [38]. This situation is possible, for example, when the stress field of the crack interacts with the stress field of another nearby crack of the equal or bigger size. Most of the studies concerning the crystallography of QC surfaces were conducted on notched single crystals [19,27]. The spatial orientation of the fracture surface was determined with respect to the crystallographic orientation of a single crystal. In this case, the major crack nucleates at the notch and propagates to the opposite side of the specimen along a low-index plane. Let us assume that growth of this crack occurs by the alternating dislocation slip from its tip. Then, indeed the propagation of the crack should occur without significant deviation from the low-index plane because the stress field at the cracks tip remains

symmetrical along the whole crack path. Although secondary cracks can nucleate around the main crack, they are much smaller, and, thus, the influence of their stress fields is not significant to cause any considerable change in the primary crack path. In contrast, the present results confirm that the path of the secondary cracks can be significantly changed due to the influence of the multiaxial stress fields created by the much larger main crack or by the closely spaced secondary cracks of equal or larger size. However, the influence of the secondary cracks seems to be less significant because the closely spaced secondary cracks apart from the main crack were not curved as much as those found in the close proximity to the main crack. The propagation paths of multiple cracks is a complex problem. Various criteria, e.g. maximum tangential stress, minimum strain energy density, maximum principal stress and energy release rate, material forces criterion, etc. have been proposed for the crack path prediction under mixed-mode loading. However, factors – both mechanical and microstructural - controlling the trajectory of the propagating crack are not completely understood as yet.

The crack path can be straight or curved, depending on the multiaxial local stress distribution, which in the simplified 2D model approach can be schematically represented as a line of the maximum stress, indicated by the red dashed line in Fig. 15. The real material cannot be considered as an elastic continuum, in general, due to microstructural inhomogeneities. The crack path is therefore intrinsically linked with the microstructure, and cannot perfectly align itself with the line of the local maximum principal stress. The quality of the agreement between the predicted and actual crack path depends not only on the criterion chosen, e.g. the maximum principal stress but also on the microstructurally influenced crack growth mechanism. Let us assume that the crack propagates by a cleavage-like mechanism along {001} planes. When one of such planes coincides with the dashed line, the crack propagates perfectly straight as shown in Fig. 15a. However, if the line of the maximum principal stress is inclined with respect to the {001} traces, the crack, which has to be aligned with the specific crystallographic plane, would tend to grow in the direction as close as possible to the line of the maximum triaxial stress, Fig. 15b. Thus, when the crack is far away from the line of the maximum stress, there is a driving force for the crack to curl out of its plane and propagate along the equal {001} plane. This produces a new facet on the fracture surface oriented at 90° to the previous one. The question is how long the cleavage crack may grow along the same crystallographic plane before turning back to the line of the maximum stress? Commonly, when the cleavage occurs in S235JR steel with 30 μm average grain size (for example during tensile testing in liquid nitrogen), the cracks seldom turn on 90° more than one time within one grain. However, during testing at low temperature, the whole specimen is embritteled, and, thus, the cleavage crack shoots easily through the entire grain. In the case of HE, the material can be brittle only in some local regions with high hydrogen concentration, for example, in the area ahead

of the crack tip. In this case, the distance of the elementary crack jump along the single plane should be not lesser than the size of the hydrogen-enriched zone. Usually, it is assumed to be about 1 μm size, which corresponds approximately to the inter-striations distance on the fracture surface [39]. Thus, the length of the straight fragment of the crack path between the 90° turns is believed to be of the order of 1 μm. Hence, the crack would appear in a triangular or sine form as shown schematically in Fig. 15b and c for the straight and curved line of the maximum stress, respectively. The step-like zig-zag appearance of the cracks, represented in Figs. 15b and c, is quite different from that is found in the present study.

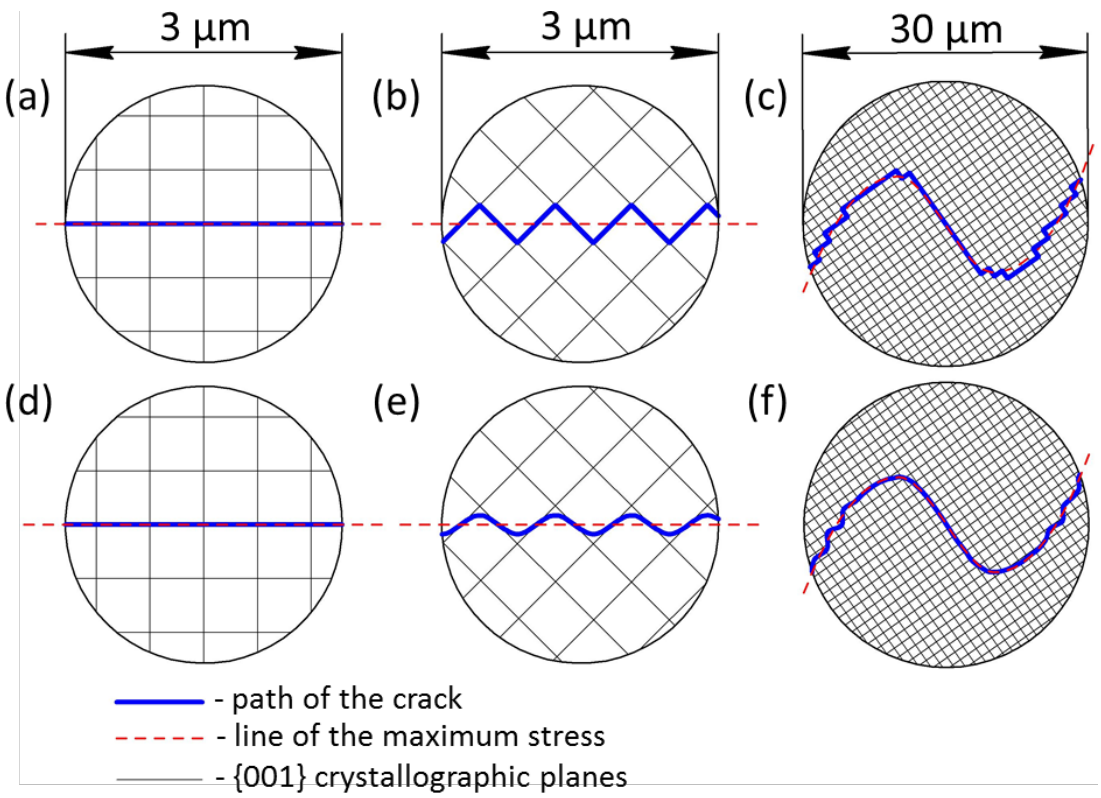

Fig. 15 – The schematic representation of the crack path on 3 (a, b, d, e) and 30 (c, d) μm scales, depending on the crystallographic orientation of the grain with respect to the line of the maximum principal stress for cleavage (a-c) and the AIDE (d-f) mechanisms of the crack growth. Scale bars of 3 and 30 μm are aimed at illustrating the approximate scale of the crack elements sizes.

Let us assume that HAC occurs along {001} planes by the dislocation emission from the crack tip. In this case, if one of the {001} planes is aligned with the plane of the maximum triaxial stress, the path of the crack is straight, just like that for cleavage, Fig. 15d. And again, typically for cleavage, when the {001} planes are inclined to the plane of maximum triaxial stress, the crack tends to turn every time when it deviates significantly from the maximum stress direction. The

steps produced by individual dislocations emerging on the surface at the crack tip are of the order of one Burgers vector. Hence, the crack kinking appears visibly much smoother than in the case of the cleavage crack on the same scale, Fig. 15e. Thereby, when the maximum stress corresponding to the uniform stress distribution is straight, the crack would have the wavy-like path with the shape similar to that of the fine cracks seen in Fig. 7f, 9f, 10a, 11a. If the stress distribution is non-uniform, i.e. the line of the maximum stress is curved somehow, Fig. 15c, the crack path would coincide with this line more accurately than that for cleavage. Nevertheless, on the local scale, it would exhibit a waviness in regions where the line of the maximum stress is inclined to {001} planes, and otherwise it would be straight wherever they coincide.

It should be noticed that the smoothly curved cracks can also be produced by other ductile mechanisms such as HELP and NVC. These mechanisms, as well as AIDE, assume the formation of nano-voids ahead of the crack. Although according to the HELP and NVC mechanisms the voids should be formed along the slip lines or their intersections, it is quite reasonable to expect that they would tend to nucleate preferably in the region of the maximum stress. The coalescence of nano-sized voids arranged along the curved line of the maximum stress could result in the formation of the crack surface with the smoothly rounded appearance on the same scale as that in Fig. 7b, 9e, 12. Nevertheless, the role of individual ductile mechanisms in HAC of low-carbon steels and iron has yet to be investigated in further studies.

5. Conclusions.

1. Hydrogen-assisted cracking resulting in the formation of fisheye defects, smoothly curved quasi-cleavage cracks and facets on the side and fracture surfaces of the low-carbon steel is mediated by the nano-void initiation and coalescence process and, thus, occurs primarily by the ductile-like mechanism.

2. The main factor controlling the propagation trajectory of the hydrogen-assisted crack is the local stress distribution while the influence of the microstructure including the crystallographic orientation of grains is less significant even for the crack propagating through an individual grain. On the local scale of the grain, the hydrogen-affected crack path may be perfectly crystallographic or may significantly deviate from the specific low-index crystallographic planes.

3. When the ex-situ hydrogen charging is performed, hydrogen-assisted cracking occurs mainly internally with the formation of fisheye defects, while the fracture of the sub-surface layer occurs primarily by the microvoid coalescence process, causing the familiar ductile dimpled fracture. In-situ hydrogen charging maintains a high concentration of hydrogen at the specimens surface and its intimate proximity promoting crack initiation at the surface. The microcracks then

propagate into the bulk producing the pure quasi-cleavage fracture surface without signatures of the ductile fracture. Thus, the in-situ charging is considered more suitable for the assessment of the HAC mechanism and related crack path by the side surface observations in the low-carbon steel.

Acknowledgements

Financial support from the Russian Foundation for Basic Research (grant-in-aid 17-08-01033) is gratefully acknowledged.

List of References

[1] M.L. Martin, J.A. Fenske, G.S. Liu, P. Sofronis, I.M. Robertson, On the formation and nature of quasi-cleavage fracture surfaces in hydrogen embrittled steels, Acta Mater. 59 (2011) 1601–1606. doi:10.1016/j.actamat.2010.11.024.

[2] S.P. Lynch, Hydrogen embrittlement phenomena and mechanisms, Corros. Rev. 30 (2012) 63–133. doi:10.1515/corrrev-2012-0502.

[3] Y. Takahashi, M. Tanaka, K. Higashida, H. Noguchi, Hydrogen-induced slip localization around a quasi-brittle fatigue crack observed by high-voltage electron microscopy, Scr. Mater. 61 (2009) 145–148. doi:10.1016/j.scriptamat.2009.03.020.

[4] F. Nakasato, I. Bernstein, Crystallographic and fractographic studies of hydrogen- induced cracking in purified iron and iron- silicon alloys, Metall. Mater. Trans. A. 9 (1978) 1317–1326. doi:10.1007/bf02652256.

[5] Y. Kikuta, T. Araki, T. Kuroda, Analysis of Fracture Morphology of Hydrogen-Assisted Cracking in Steel and Its Welds, in: B.M. Strauss, W.H. Cullen (Eds.), Fractography Fail. Anal., 1978: pp. 107–127. doi:10.1520/STP38088S.

[6] C.D. Beachem, Orientation of cleavage facets in tempered martensite (quasi-cleavage) by single surface trace analysis, Metall. Trans. 4 (1973) 1999–2000. doi:10.1007/BF02665434.

[7] A. Kumar, A.J. Wilkinson, S.G. Roberts, Quasi-cleavage fracture planes in spheroidized

A533B steel, J. Microsc. 227 (2007) 248–253. doi:10.1111/j.1365-2818.2007.01808.x.

[8] S.Y. Jo, J. Han, J.-H. Kang, S. Kang, S. Lee, Y.-K. Lee, Relationship between grain size and ductile-to-brittle transition at room temperature in Fe-18Mn-0.6C-1.5Si twinning-induced plasticity steel, J. Alloys Compd. 627 (2015) 374–382. doi:10.1016/j.jallcom.2014.11.232.

[9] R.L. Tobler, D. Meyn, Cleavage-like fracture along slip planes in Fe-18Cr-3Ni-13Mn-0.37N austenitic stainless steel at liquid helium temperature, Metall. Trans. A. 19 (1988) 1626–1631. doi:10.1007/BF02674040.

[10] C.D. Beachem, R.M.N. Pelloux, Electron Fractography—A Tool for the Study of Micromechanisms of Fracturing Processes, in: A.C. E-24 (Ed.), Fract. Toughness Test. Its Appl., 1965: pp. 210–244.

[11] E. Merson, A.V. Kudrya, V.A. Trachenko, D. Merson, V. Danilov, A. Vinogradov, Quantitative characterization of cleavage and hydrogen-assisted quasi-cleavage fracture surfaces with the use of confocal laser scanning microscopy, Mater. Sci. Eng. A. 665 (2016) 35–46. doi:10.1016/j.msea.2016.04.023.

[12] T.J. Marrow, M. Aindow, P. Prangnell, M. Strangwood, J.F. Knott, Hydrogen-assisted stable crack growth in iron-3 wt% silicon steel, Acta Mater. 44 (1996) 3125–3140. doi:10.1016/1359-6454(95)00429-7.

[13] X. Chen, W.W. Gerberich, Evidence for 1μm size instabilities in hydrogen-assisted cracking of Fe3%Si crystals, Scr. Metall. 22 (1988) 1499–1502. doi:10.1016/S0036-9748(88)80027-9.

[14] E.D. Merson, P.N. Myagkikh, G.V. Klevtsov, D.L. Merson, A. Vinogradov, Effect of fracture mode on acoustic emission behavior in the hydrogen embrittled low-alloy steel, Eng. Fract. Mech. 210 (2019) 342–357. doi:10.1016/j.engfracmech.2018.05.026.

[15] M.L. Martin, M. Dadfarnia, A. Nagao, S. Wang, P. Sofronis, Enumeration of the hydrogen-enhanced localized plasticity mechanism for hydrogen embrittlement in structural materials, Acta Mater. 165 (2019) 734–750. doi:10.1016/j.actamat.2018.12.014.

[16] I.M. Robertson, P. Sofronis, A. Nagao, M.L. Martin, S. Wang, D.W. Gross, et al., Hydrogen Embrittlement Understood, Metall. Mater. Trans. A. 46 (2015) 2323–2341. doi:10.1007/s11661-015-2836-1.

[17] T. Neeraj, R. Srinivasan, J. Li, Hydrogen embrittlement of ferritic steels: Observations on deformation microstructure, nanoscale dimples and failure by nanovoiding, Acta Mater. 60 (2012) 5160–5171. doi:http://dx.doi.org/10.1016/j.actamat.2012.06.014.

[18] M. Nagumo, Hydrogen Embrittlement: Theories, in: R. Colás, G.E. Totten (Eds.), Encycl. Iron, Steel, Their Alloy., Taylor & Francis, 2016: pp. 1785–1800. doi:10.1081/E-EISA-120049350.

[19] X. Chen, W.W. Gerberich, The Kinetics and Micromechanics of Hydrogen- Assisted Cracking in Fe-3 Pct Si Single Crystals, Metall. Trans. A. 22 (1991) 59–70. doi:10.1007/BF03350949.

[20] J. Song, W. a Curtin, Atomic mechanism and prediction of hydrogen embrittlement in iron., Nat. Mater. 12 (2012) 145–51. doi:10.1038/nmat3479.

[21] A.. Tetelman, W.. Robertson, Direct observation and analysis of crack propagation in iron-3% silicon single crystals, Acta Metall. 11 (1963) 415–426. doi:10.1016/0001-6160(63)90166-4.

[22] W.W. Gerberich, R.H. Jones, M.A. Friesel, A. Nozue, Acoustic emission monitoring of stress corrosion cracking, Mater. Sci. Eng. A. 103 (1988) 185–191. doi:10.1016/0025-5416(88)90565-4.

[23] S.P. Lynch, Environmentally assisted cracking: Overview of evidence for an adsorption-induced localised-slip process, Acta Metall. 36 (1988) 2639–2661. doi:10.1016/0001-6160(88)90113-7.

[24] I.M. Bernstein, Hydrogen-induced cracking in iron: Morphology and crack path dependence, Metall. Trans. 1 (1970) 3143–3150. doi:10.1007/BF03038430.

[25] I.M. Bernstein, The role of hydrogen in the embrittlement of iron and steel, Mater. Sci. Eng. 6 (1970) 1–19. doi:10.1016/0025-5416(70)90073-x.

[26] A. Kimura, H. Kimura, Hydrogen embrittlement in high purity iron single crystals, Mater. Sci. Eng. 77 (1986) 75–83. doi:10.1016/0025-5416(86)90355-1.

[27] N. Takano, K. Kidani, Y. Hattori, F. Terasaki, Fracture surface of hydrogen embrittlement in iron single crystals, Scr. Metall. Mater. 29 (1993) 75–80. doi:10.1016/0956-716X(93)90257-S.

[28] D. Birenis, Y. Ogawa, H. Matsunaga, O. Takakuwa, J. Yamabe, Ø. Prytz, et al., Hydrogen-assisted fatigue crack propagation in a pure BCC iron. Part II: Accelerated regime manifested by quasi-cleavage fracture at relatively high stress intensity range values, MATEC Web Conf. 165 (2018) 03010. doi:10.1051/matecconf/201816503010.

[29] D. Birenis, Y. Ogawa, H. Matsunaga, O. Takakuwa, J. Yamabe, Ø. Prytz, et al., Interpretation of hydrogen-assisted fatigue crack propagation in BCC iron based on dislocation structure evolution around the crack wake, Acta Mater. 156 (2018) 245–253. doi:10.1016/j.actamat.2018.06.041.

[30] K. Okada, A. Shibata, Y. Takeda, N. Tsuji, Crystallographic feature of hydrogen-related fracture in 2Mn-0.1C ferritic steel, Int. J. Hydrogen Energy. 43 (2018) 11298–11306. doi:10.1016/j.ijhydene.2018.05.011.

[31] E. Merson, A. Vinogradov, D.L. Merson, Application of acoustic emission method for investigation of hydrogen embrittlement mechanism in the low-carbon steel, J. Alloys Compd. 645 (2015) S460–S463. doi:10.1016/j.jallcom.2014.12.083.

[32] A. Griesche, E. Dabah, T. Kannengiesser, N. Kardjilov, A. Hilger, I. Manke, Three-dimensional imaging of hydrogen blister in iron with neutron tomography, Acta Mater. 78 (2014) 14–22. doi:10.1016/j.actamat.2014.06.034.

[33] A. Laureys, T. Depover, R. Petrov, K. Verbeken, Influence of sample geometry and microstructure on the hydrogen induced cracking characteristics under uniaxial load, Mater. Sci. Eng. A. 690 (2017) 88–95. doi:10.1016/j.msea.2017.02.094.

[34] J.Y. Lee, J.L. Lee, A trapping theory of hydrogen in pure iron, Philos. Mag. A. 56 (1987) 293–309. doi:10.1080/01418618708214387.

[35] M.C. Tiegel, M.L. Martin, A.K. Lehmberg, M. Deutges, C. Borchers, R. Kirchheim, Crack and blister initiation and growth in purified iron due to hydrogen loading, Acta Mater. 115 (2016) 24–34. doi:10.1016/j.actamat.2016.05.034.

[36] A. Laureys, E. Van den Eeckhout, R. Petrov, K. Verbeken, Effect of deformation and charging conditions on crack and blister formation during electrochemical hydrogen charging, Acta Mater. 127 (2017) 192–202. doi:10.1016/j.actamat.2017.01.013.

[37] E.D. Merson, Study of the Fracture Mechanism and Acoustic Emission Nature at the Hydrogen Embrittlement of the Low-Carbon Steel, Togliatti State University, 2016.

http://misis.ru/files/3833/Merson_ED_disser.pdf.

[38] S.P. Lynch, A fractographic study of hydrogen-assisted cracking and liquid-metal embrittlement in nickel, J. Mater. Sci. 21 (1986) 692–704. doi:10.1007/bf01145543.

[39] W. Gerberich, Modeling hydrogen induced damage mechanisms in metals, in: R.P. Gangloff, B.P. Somerday (Eds.), Gaseous Hydrog. Embrittlement Mater. Energy Technol. Vol. 2 Mech. Model. Futur. Dev., Woodhead Publishing Limited, Philadelphia, 2012: pp. 209–246. doi:10.1016/B978-0-85709-536-7.50008-8.